2011 American Control Conference
on O'Farrell Street, San Francisco, CA, USA
June 29 - July 01, 2011

Robust Estimation of Road Friction Coefficient

Changsun Ahn, Huei Peng, and H. Eric Tseng

Abstract— **Vehicle active safety systems stabilize the vehicle by controlling tire forces. They work well only when the commanded tire forces are within the friction limit. Therefore, knowledge of the tire/road friction is important to improve the performance of vehicle active safety systems. This paper presents two methods to estimate the friction coefficient: one based on lateral dynamics, and one based on longitudinal dynamics. The two methods are then integrated to improve working range of the estimator and robustness. The first method is a nonlinear observer based on vehicle lateral/yaw dynamics and Brush Tire model, the second method is a recursive least squares method based on the relationship between tire longitudinal slip and traction force. The performance of the estimation algorithm is verified using test data under a wide range of friction and speed conditions.**

I. Introduction

TIRE-road friction influences the ability of tires to generate steering, traction, and braking forces and thus affects vehicle motion. Knowledge of the friction coefficient of the road is thus important for the design and analysis of vehicle control systems, especially active safety systems. When friction is unknown, the design is usually conservative, resulting in reduced performance.

Many approaches to estimate tire-road friction have been proposed based on different dynamics and phenomena. The approaches can be categorized into cause-based and effect-based methods. Cause-based methods [1-3] detect materials covering road surfaces, such as water, ice, and snow, by using vision, temperature or other sensors. These methods can estimate the friction coefficient of the road ahead which can be beneficial. However, they usually do not manifest other factors affecting friction, such as tire conditions. The effect-based methods utilize vehicle and tire dynamic behaviors directly, e.g., the relationship between tire slip ratio and longitudinal force [4-6], wheel speed frequency content [7], vehicle lateral dynamics [8-11], and front tire aligning moment [12, 13].

Vehicle lateral dynamics is more robust to high frequency disturbances than tire-based methods because the vehicle lateral dynamics are low-pass by nature. Furthermore, the measurement of front tire aligning moment is readily available in vehicles equipped with Electronic Stability Control (ESC), Electronic Power Assisting System (EPAS), and Active Front Steering (AFS). However, quite often in daily driving, significant level of lateral excitation does not exist. Longitudinal tire force based methods then must be used. The availability of required sensors and the straightforward force-friction coefficient relationship are two key benefits of longitudinal dynamics based methods.

In the authors' previous papers [14, 15], an algebraic and a dynamic estimator were developed based on lateral dynamics and front tire aligning moment. The estimator achieves good performance under nominal conditions. In a subsequent paper [16], the dynamic method is improved and a synthesis method for robust performance is presented. In this paper, we enhance the previous method by developing a longitudinal dynamics based estimator and integrate it with the lateral-dynamics based method. The integrated estimator increases the working ranges of the estimators. The integrated algorithm is verified by vehicle tests on several surfaces.

II. Lateral Dynamics Based Method

A. Observer Design Synthesis

The synthesis process proposed in [16] is summarized below. A nonlinear system with an unknown state and a parameter is expressed as

$$\dot{x} = f(x,u,\theta), \quad y = \begin{bmatrix} y_1 \\ y_2 \end{bmatrix} = \begin{bmatrix} h_1(x,u,\theta) \\ h_2(x,u,\theta) \end{bmatrix}, \tag{1}$$

For which an observer can be designed:

$$\begin{aligned} \dot{\hat{x}} &= f(\hat{x},u,\hat{\theta}) + L_{11}(y_1 - \hat{y}_1) + L_{12}(y_2 - \hat{y}_2), \\ \dot{\hat{\theta}} &= L_{21}(y_1 - \hat{y}_1) + L_{22}(y_2 - \hat{y}_2), \end{aligned} \tag{2}$$

where

$$\begin{aligned} L_{11} &= \left(k_1 \frac{\partial h_1}{\partial x} + \frac{\partial f}{\partial x} \Big/ \frac{\partial h_1}{\partial x} \right)_{x=\hat{x},\theta=\hat{\theta}}, \; L_{12} = k_2 \left(\frac{\partial h_2}{\partial x} \right)_{x=\hat{x},\theta=\hat{\theta}}, \\ L_{21} &= k_3 \left(\frac{\partial h_1}{\partial \theta} \right)_{x=\hat{x},\theta=\hat{\theta}}, \; L_{22} = k_4 \left(\frac{\partial h_2}{\partial \theta} \right)_{x=\hat{x},\theta=\hat{\theta}}, \end{aligned} \tag{3}$$

and $k_1 \sim k_4$ can be determined using a optimization routine that maximizes robust stability against plant uncertainties.

Manuscript received September 27, 2010. This work was supported by Ford Motor Company.

C. Ahn is a research fellow in the Department of Mechanical Engineering, University of Michigan, Ann Arbor, MI 48109-2133, USA (phone: 734-647-9732; e-mail: sunahn@umich.edu).

H. Peng is a professor of the Department of Mechanical Engineering, University of Michigan, Ann Arbor, MI 48109-2133, USA (e-mail: hpeng@umich.edu).

H. E. Tseng is a technical leader of the Powertrain Controls Research & Advanced Engineering, Ford Motor Company, Dearborn, MI 48121 USA (e-mail: htseng@ford.com).

B. System Models for Lateral Dynamics

The lateral dynamics model is a standard bicycle model. Derivation of the equations of motion for the bicycle model follows from the force and moment balance:

$$m(\dot{v}_y + v_x r) = F_{yf} + F_{yr}, \quad I_z \dot{r} = aF_{yf} - bF_{yr}, \tag{4}$$

where v_x is the vehicle forward speed, v_y is the vehicle lateral speed, r is the yaw rate, m is the vehicle mass, and I_z is the yaw moment of inertia. F_{yf} is the lateral force at the front axle and F_{yr} is the lateral forces at the rear axles. δ is the front wheel steering angle, and a and b are the distance from vehicle center of gravity to front and rear axles. Taking small angle approximations, the tire slip angles α_f and α_r are calculated from:

$$\alpha_f = (v_y + ar)/v_x - \delta, \quad \alpha_r = (v_y - br)/v_x. \tag{5}$$

The Brush Tire model is selected because it uses few parameters and captures fundamental nonlinear tire behavior. In the Brush Tire model, the lateral tire force and the tire self-aligning torque are calculated from:

$$\begin{cases} F_y = -3\mu F_z \rho_y \left(1 - |\rho_y| + \frac{1}{3}\rho_y^2\right) \\ \tau_a = \mu F_z c \rho_y \left(1 - |\rho_y|\right)^3 \end{cases}, \quad for\ |\alpha| \le |\alpha_{sl}|,$$
$$\begin{cases} F_y = -\mu F_z sgn(\alpha) \\ \tau_a = 0 \end{cases}, \quad for\ |\alpha| > |\alpha_{sl}|, \tag{6}$$

where $\alpha_{sl} = \tan^{-1}(1/\theta_y)$, $\theta_y = 2c_p l^2/(3\mu F_z)$, $\rho_y = \theta_y \sigma_y$, $\sigma_y = \tan(\alpha)$, l is half of tire contact length, α is the tire slip angle, μ is the tire-road friction coefficient, F_z is the tire normal force, and c_p is the tread stiffness in unit length.

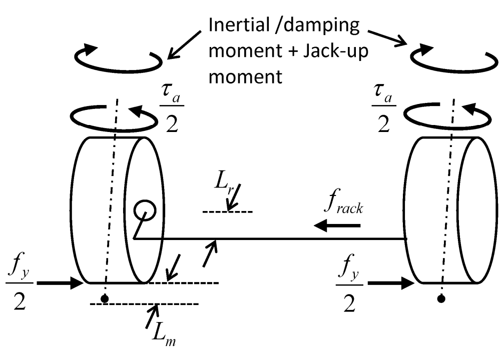

Fig. 1. Steering system dynamics

Finally, the steering system in Fig. 1 is described by:

$$J_{eff}\ddot{\delta} + b_{eff}\dot{\delta} + k\delta = \tau_a + f_y \cdot L_m - f_{rack} \cdot L_r, \tag{7}$$

where δ is a road steer angle, J_{eff} is the effective moment of inertia, b_{eff} is the effective damping of the steering system, and k is the jack-up moment coefficient τ_a is the self-aligning moment of the tire. The jack-up moment is the moment caused by the returning tendency of the lifted vehicle body when steering angle increases.

C. Observer Design

From (4) and (5), we have:

$$\dot{\alpha}_f = \left(\frac{1}{mv_x} + \frac{a^2}{I_z v_x}\right)F_{yf} + \left(\frac{1}{mv_x} - \frac{ab}{I_z v_x}\right)F_{yr} - r - \dot{\delta}. \tag{8}$$

where F_{yf} and F_{yr} are functions of the state α_f and the unknown parameter μ. We assume that tire normal force F_z can be achieved from vehicle mass and a load transfer model. The two measurements are

$$y = \begin{bmatrix} ma_y & f_{rack} \end{bmatrix}^T. \tag{9}$$

where a_y is the vehicle lateral acceleration measured by a G-sensor, and f_{rack} is the steering rack force measured by strain gauges. Then the observer designed by the synthesis is

$$\begin{aligned} \dot{\hat{\alpha}}_f &= \left(\frac{1}{mv_x} + \frac{a^2}{I_z v_x}\right)\hat{F}_{yf} + \left(\frac{1}{mv_x} - \frac{ab}{I_z v_x}\right)\hat{F}_{yr} - r - \dot{\delta} \\ &\quad + L_{11}\left(ma_y - \left(\hat{F}_{yf} + \hat{F}_{yr}\right)\right) + L_{12}\left(f_{rack} - \hat{f}_{rack}\right), \\ \dot{\hat{\mu}} &= L_{21}\left(ma_y - \left(\hat{F}_{yf} + \hat{F}_{yr}\right)\right) + L_{22}\left(f_{rack} - \hat{f}_{rack}\right), \end{aligned} \tag{10}$$

where $\hat{f}_{rack} = \left[\hat{\tau}_a + \hat{f}_y \cdot L_{mr} - \left(J_{eff}\ddot{\delta} + b_{eff}\dot{\delta} + k\delta\right)\right]/L_r$.

The observer gain can be achieved by (3) with the following parameters obtained through the optimization process [16]:

$$k_1 = 2.5\times10^{-9},\ k_2 = 2.8\times10^{-6},\ k_3 = 1.8\times10^{-8},\ k_4 = 1.9\times10^{-4}.$$

The detail for observer gain optimization can be found in [16].

III. Longitudinal Dynamics Based Method

A. Estimator Design

Longitudinal excitations are almost always present in daily driving. When driving on straight roads, lateral excitations may not be present, and road friction can only be manifested through longitudinal dynamics. Longitudinal excitations are generally quite small (less than few % of longitudinal slip). Under these cases, the basis of estimation is longitudinal tire stiffness in the small slip region. Physics based tire models such as the Brush Tire model, predict that the longitudinal stiffness is independent of road surfaces in small slip region. However, in the literature, several experimental results show that longitudinal stiffness depends on the friction coefficient and the phenomenon has been used for road friction estimation [17-20]. Our experimental results also show that tire force is dependent on friction level at small slip ratio, as shown in Fig. 2.

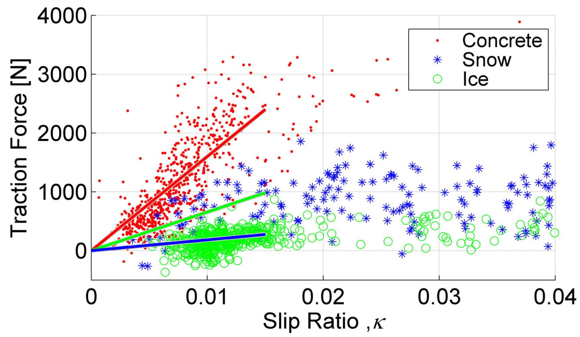

Fig. 2. Experimental results at small longitudinal slip

In the small-slip region, the longitudinal force can be expressed as follows:

$$F_x(\kappa) \approx k(\mu)\cdot\kappa, \; for \; |\kappa| < 0.015, \tag{11}$$

The longitudinal stiffness $k(\mu)$ depends on the tire characteristics but it also changes with friction level μ. The friction coefficients and longitudinal stiffness between a tire (in our Jaguar S-type test vehicle, the Pirelli 255/50R-17) and three surfaces are listed in Table I. Equation (11) can be rewritten as a standard parameter identification form:

$$y(t) = \varphi^T(t)\theta(t), \tag{12}$$

where the output $y(t)=F_x$, the unknown parameter $\theta(t)=k(\mu)$, and the measured slip ratio $\varphi(t)=\kappa$. Once the stiffness $k(\mu)$ is identified, the friction coefficient can be calculated through interpolation using data in Table I.

B. Recursive Least Squares (RLS)

The recursive least squares method [21] iteratively updates the unknown parameter at each sampling time to minimize the sum of the squares of the modeling error, using the past data within the regression vector, $\varphi(t)$. The general synthesis of RLS algorithm is as follows:

Step 0: Initialize the unknown parameter $\theta(0)$ and the covariance matrix $P(0)$; select forgetting factor λ.

Step 1: Measure the system output $y(t)$ and compute the regression vector $\varphi(t)$.

Step 2: Calculate the identification error $e(t)$:

$$e(t) = y(t) - \varphi^T(t)\theta(t-1). \tag{13}$$

Step 3: Calculate the gain $K(t)$:

$$K(t) = P(t-1)\varphi(t)\left[\lambda + \varphi(t)^T P(t-1)\varphi(t)\right]^{-1}. \tag{14}$$

Step 4: Calculate the covariance matrix:

$$P(t) = \lambda^{-1}P(t-1) - K(t)\varphi(t)^T\lambda^{-1}P(t-1). \tag{15}$$

Step 5: Update the unknown parameter:

$$\theta(t) = \theta(t-1) + K(t)e(t). \tag{16}$$

Step 6: Repeat Steps 1~5 for each sampling time.

TABLE I
FRICTION COEFFICIENT AND LONGITUDINAL STIFFNESS OF A TIRE ON SEVERAL SURFACES

Road Surface	Friction Coefficient	Longitudinal Stiffness
Concrete	0.85~1.0	16.0×10^4
Snow	0.35~0.4	6.6×10^4
Ice	0.15~2	1.8×10^4

C. Stiffness Identification

For a rear-wheel drive vehicle, the standard form of parameter identification can be expressed as:

$$ma_x = F_{x,rl} + F_{x,rr} - D, \tag{17}$$

where $D=C_{drag}\cdot A\cdot\rho\cdot v_x^2/2$ is the air drag, A is the cross-section area of the vehicle, and ρ is the air density. Using the linear tire force model shown in (11), (17) can be rewritten as:

$$a_x + \frac{D}{m} = \frac{\kappa_{rl}+\kappa_{rr}}{m}K(\mu). \tag{18}$$

We can then identify the stiffness $K(\mu)$ if an RLS problem is defined with $y(t) = a_x+D/m$, $\varphi(t)=(\kappa_{rl}+\kappa_{rr})/m$, and $\theta(t)=K(\mu)$.

IV. INTEGRATED ALGORITHM

The lateral dynamics and longitudinal dynamics based algorithms described above are used to create an integrated estimator, the switching between the two methods relies on the nature and magnitude of excitations. The lateral dynamics based method is useful under medium lateral excitations, and the longitudinal dynamics based method works when there is no lateral excitation and slip ratio less than 2%. In Fig. 3, the covered region of the two methods is shown. They were both developed based on pure slip cases. Their performance under the combined slip cases cannot be guaranteed, and in fact we expect poor performance due to tire nonlinearities. To handle combined slip cases, we need to modify the underlying models.

The brush model with combined slip is as follows[22]:

$$F_x = F\frac{\sigma_x}{\sigma},\; F_y = F\frac{\sigma_y}{\sigma},\; M_z = -t(\sigma)\cdot F_y, \tag{19}$$

where

$$F(\alpha,\kappa,\mu) = \begin{cases} \mu F_z(1-\lambda^3) & for \; |\sigma| \le |\sigma_{sl}| \\ \mu F_z sgn(\alpha) & for \; |\sigma| > |\sigma_{sl}| \end{cases},$$

$$\lambda = 1-\theta\sigma,\ \ \theta = 2c_p l^2/(3\mu F_z),\ \ \sigma=\sqrt{\sigma_x^2+\sigma_y^2},$$
$$\sigma_x = \kappa/(\kappa+1),\ \ \sigma_y=(\tan\alpha)/(\kappa+1),\ \ \sigma_{sl}=1/\theta,$$
$$t(\sigma)=l\left(1-|\theta\sigma|\right)^3/\left(3-3|\theta\sigma|+|\theta\sigma|^2\right).$$

To handle the difference between the longitudinal tire forces on left and right sides, the dynamics of the vehicle model shown in Fig. 4 is modified as follows:

$$\begin{aligned} m\left(\dot{v}_y+v_x r\right) &= F_{yf}+F_{yr}, \\ I_z\dot{r} &= aF_{yf}-bF_{yr}+\frac{w}{2}F_{xr}-\frac{w}{2}F_{xl}. \end{aligned} \tag{20}$$

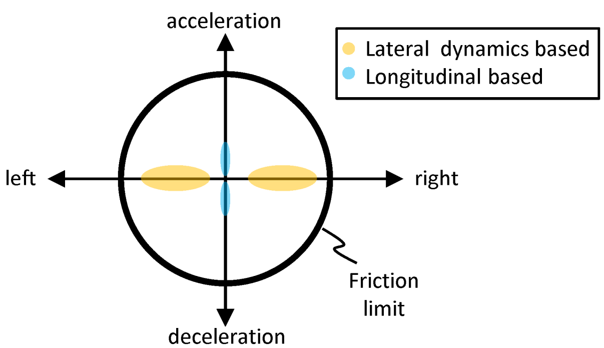

Fig.3. Coverage of the two pure-slip estimation methods

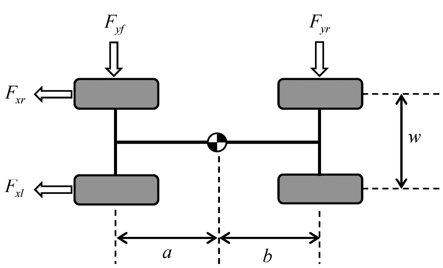

Fig. 4. Vehicle model for the combined slip case

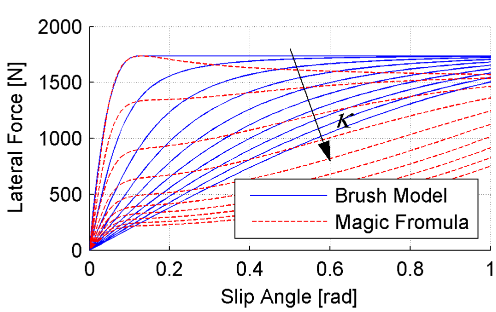

Fig. 5. Lateral force differences between Brush model and Magic formula tire model when longitudinal slip is large.

The combined slip brush model represents the real tire behavior when the slip is small. But when the combined slip is large, predicted and measured forces show large discrepancy, as shown in Fig. 5. It is difficult to model tire forces at large slip because they are affected by vertical tire forces, effect of suspension, tire structure, etc. Therefore, model error is unavoidable in large longitudinal slip cases. Instead of reducing the model discrepancy, we aim to reduce the effect of discrepancy. One way to do so is to reduce the magnitude of observer gains during high combined slip. Because the measurement model consists of the tire model, by reducing the observer gain magnitude we can reduce the effect of tire model error in the measurement model. The modified observer with the modified tire model, vehicle model, and adaptive gain to longitudinal slip is shown in the following:

$$\begin{aligned} \dot{\hat{\alpha}}_f &= \left(\frac{1}{mv_x}+\frac{a^2}{I_z v_x}\right)\hat{F}_{yf}+\left(\frac{1}{mv_x}-\frac{ab}{I_z v_x}\right)\hat{F}_{yr} \\ &\quad +\frac{w}{2I_z V_x}(\hat{F}_{xr}-\hat{F}_{xl})-r-\dot{\delta} \\ &\quad +L_{11}\left(ma_y-\left(\hat{F}_{yf}+\hat{F}_{yr}\right)\right)+L_{12}\left(f_{rack}-\hat{f}_{rack}\right), \\ \dot{\hat{\mu}} &= k_{slip}\cdot l_3\left(ma_y-\left(\hat{F}_{yf}+\hat{F}_{yr}\right)\right)+k_{slip}\cdot l_4\left(\tau_a-\hat{\tau}_a\right). \end{aligned} \tag{21}$$

where k_{slip} is the scale-down coefficient which can be tuned heuristically based on the slip ratio.

The two methods described earlier are integrated by a switching rule that is based on level of excitation. The excitation indices are normalized front tire slip angle and longitudinal slip ratio. The activation condition of the lateral dynamics based method is that the normalized slip angle should be between 0.1 and 0.7. The activation condition for the small slip ratio method is that both of rear wheels' slip ratio should be less than 1.5%, which is from Fig. 2. Using the conditions, overall estimation flow of the integrated estimator is shown in Fig. 6. If neither methods are selected, an open-loop observer will be used, in which case the feedback terms in (20) are set to zero, i.e., the slip angle is updated based on vehicle dynamics and the friction coefficient is kept constant.

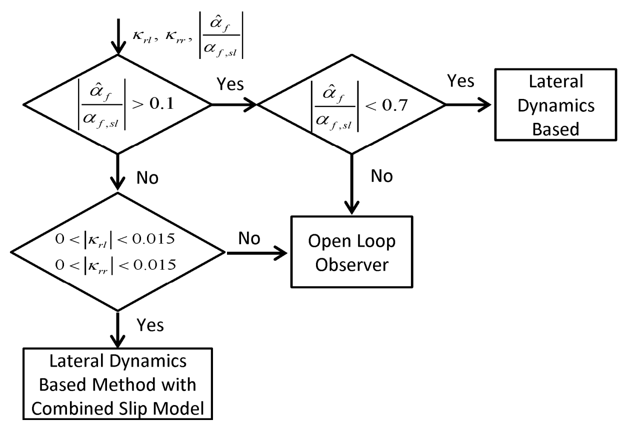

Fig. 6. Flow chart of the integrated estimator

The method used to handle the combined slip cases increases the coverage of lateral dynamics based method, as shown in Fig. 7. A common driving condition is medium range of longitudinal acceleration or deceleration with little lateral excitation. These cases can be dealt with by examining the input/output relations of ABS system, which is beyond the scope of this paper.

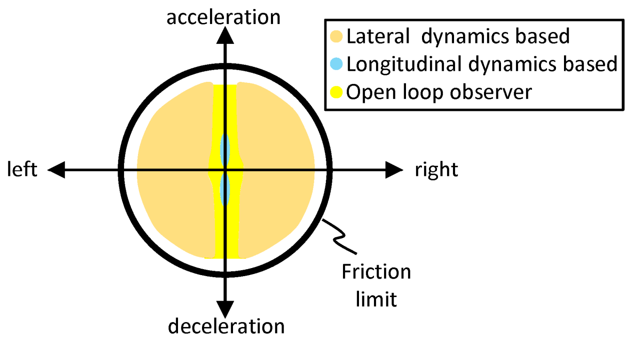

Fig. 7. Increased coverage of estimators

V. Experimental Validation

A. Experimental vehicle

Validation of the developed algorithms is performed on the winter test track of Ford Motor Company in Sault Ste. Maire, Michigan, USA. The test vehicle is a rear wheel drive Jaguar S-type, which is modified for the development of vehicle dynamics control algorithms. The vehicle has standard ESC sensors, including yaw rate and lateral acceleration sensors, four wheel speed sensors, a steering wheel angle sensor, and a steering torque sensor. For the rack force measurement, two strain gauges are installed on the steering racks. Fig. 8 shows the test vehicle and the GPS/INS system.

Fig. 8. The test vehicle and GPS/INS system

To provide reference vehicle states, an Oxford Technology RT-2500 system is installed, which has two antenna GPS integrated with INS and measures three dimensional vehicle position and orientation as well as three dimensional linear and angular velocities of the vehicle.

B. Vehicle and Tire Parameter Identification

The vehicle parameters are obtained from vehicle design specifications; however, the tire parameters are not available; therefore and need to be identified through bench tests and vehicle tests. We performed steady state turning maneuvers to identify tire stiffness and the length of the contact patch. The steering system parameters, such as the rotational inertia and the damping coefficient are identified through transient maneuvers. Finally, a transient maneuver with sinusoidal steering inputs is performed for the purpose of verification of the vehicle and tire models.

The identified parameters of the system models are evaluated by comparison between the signals from measurement and the model. Fig. 8 shows the tire model validation and Fig. 9 shows the validation of the vehicle model integrated with the identified tire and steering system models.

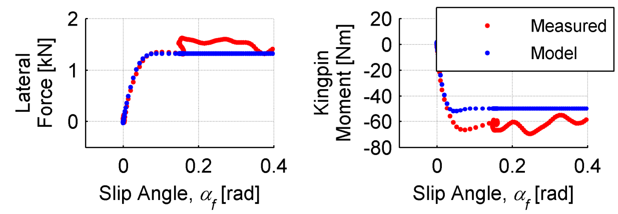

Fig. 8. Model vs. measured tire forces when vehicle is in quasi-steady state driving on snow surface

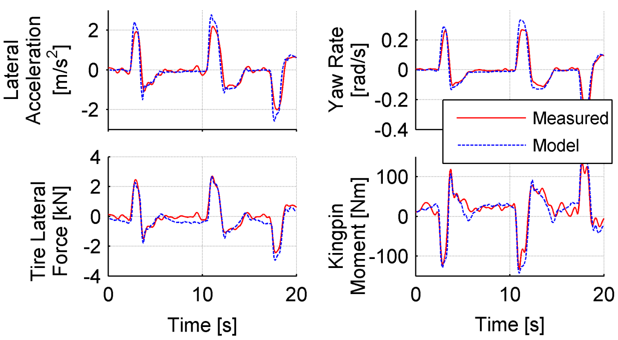

Fig. 9. Vehicle model validation using transient maneuvers on snow, vehicle speed = 25 km/h

C. Experimental Results

The test car traveled on four different surfaces: concrete, ice, snow and slippery concrete surfaces, as shown in Fig. 10. The driver intentionally performed continuous sinusoidal steering to generate lateral excitation.

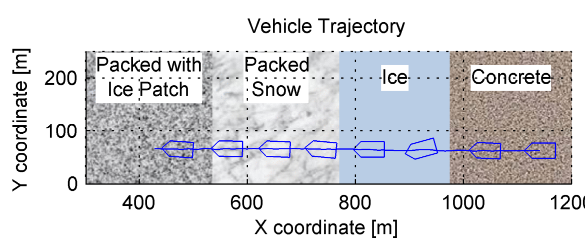

Fig. 10. Road surface of the test track

The test data for evaluation are plotted in Fig. 11 and estimation results are shown in Fig. 12. The longitudinal dynamics based algorithm shows poor performance due to infrequent longitudinal excitations. The lateral dynamics based algorithm generally tracks well the true friction coefficient except during abrupt changes. The combination of the two algorithms improves the tracking performance significantly.

The experimental results indicate that the proposed approach estimates slip angle and friction efficient but sometimes after a noticeable delay. Significant development effort is still needed to validate its robust performance.

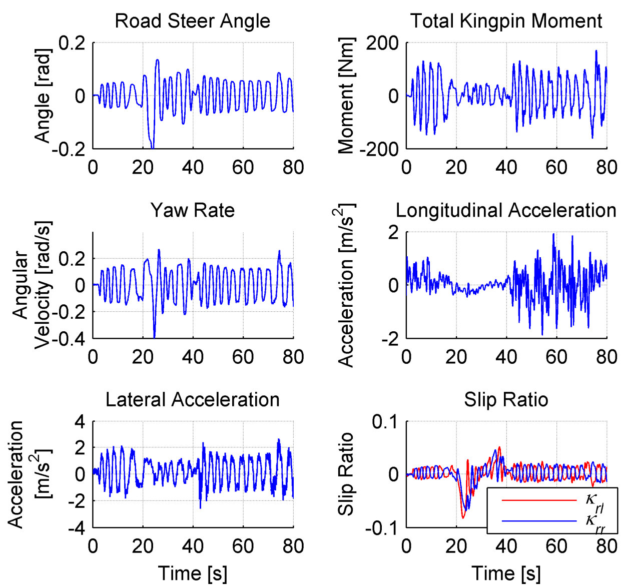

Fig. 11. Example test data under sinusoidal steering input at 30 km/h

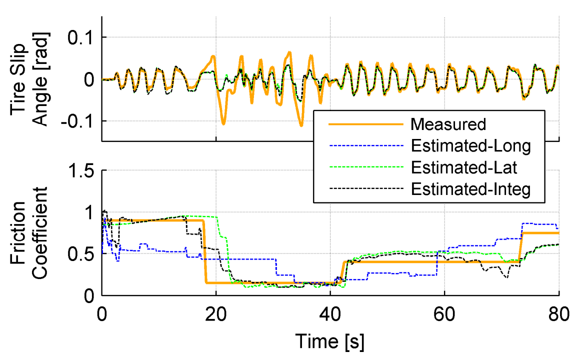

Fig. 12. Estimation results under sinusoidal steering input at 30 km/h

VI. Conclusion

This paper presents an observer for robust estimation of road friction coefficient and vehicle side slip angle. We integrate two methods each developed based on pure-slip excitations. The first estimator is based on a robust nonlinear observer methodology and vehicle lateral dynamics. The second estimator is designed using recursive least squares and longitudinal dynamics. The two methods are integrated by a switching rule. The performance of the integrated algorithm is verified through experiments. The algorithm works well under sudden surface changes and varying steering excitations. One limitation of the proposed method arises from the fact that one of the estimators is developed based on a small longitudinal slip model so that it cannot handle large longitudinal slip cases. This drawback is left for future studies.

References

[1] M. Yamada, K. Ueda, I. Horiba, S. Tsugawa, and S. Yamamoto, "Road surface condition detection technique based on image taken by camera attached to vehicle rearview mirror," *Review of Automotive Engineering,* vol. 26, pp. 163-168, 2005.

[2] F. Holzmann, M. Bellino, R. Siegwart, and H. Bubb, "Predictive estimation of the road-tire friction coefficient," in *IEEE International Conference on Control Applications*, Munich, Germany, 2006, pp. 885-890.

[3] Y. Sato, A. D. Kobay, I. Kageyama, K. Watanabe, Y. Kuriyagawa, and Y. Kuriyagawa, "Study on recognition method for road friction condition," *JSAE Transaction,* vol. 38, pp. 51-56, 2007.

[4] C.-S. Liu and H. Peng, "Road friction coefficient estimation for vehicle path prediction," *Vehicle System Dynamics,* vol. 25, pp. 413 - 425, 1996.

[5] M. Ito, K. Yoshioka, and T. Saji, "Estimation of road surface conditions using wheel speed behavior," in *International Symposium on Advanced Vehicle Control*, Tsukuba, Japan, 1994, pp. 533-538.

[6] F. Gustafsson, "Monitoring tire-road friction using the wheel slip," *IEEE Control Systems Magazine,* vol. 18, pp. 42-49, 1998.

[7] T. Umeno, E. Ono, Katsuhiro, S. Ito, A. Tanaka, Yoshiyuki, and M. Sawada, "Estimation of tire-road friction using tire vibration model," presented at the SAE 2002, Detroit, Michigan, USA, 2002.

[8] C. Sierra, E. Tseng, A. Jain, and H. Peng, "Cornering stiffness estimation based on vehicle lateral dynamics," *Vehicle System Dynamics,* vol. 44, pp. 24 - 38, 2006.

[9] J.-O. Hahn, R. Rajamani, and L. Alexander, "GPS-based real-time identification of tire-road friction coefficient," *IEEE Transactions on Control Systems Technology,* vol. 10, pp. 331-343, 2002.

[10] W. R. Pasterkamp and H. B. Pacejka, "The tyre as a sensor to estimate friction," *Vehicle System Dynamics,* vol. 27, pp. 409 - 422, 1997.

[11] L. R. Ray, "Nonlinear tire force estimation and road friction identification: simulation and experiments," *Automatica,* vol. 33, pp. 1819-1833, 1997.

[12] Y. Yasui, W. Tanaka, Y. Muragishi, E. Ono, M. Momiyama, H. Katoh, H. Aizawa, and Y. Imoto, "Estimation of lateral grip margin based on self-aligning torque for vehicle dynamics enhancement," presented at the SAE 2004, Detroit, Michigan, USA, 2004.

[13] Y.-H. J. Hsu and J. C. Gerdes, "A feel for the road: A method to estimate tire parameters using steering torque," in *International Symposium on Advanced Vehicle Control*, Taipei, Taiwan, 2006.

[14] C. Ahn, H. Peng, and H. E. Tseng, "Estimation of road friction for enhanced active safety systems: Algebraic approach," in *American Control Conference, 2009*, 2009, pp. 1104-1109.

[15] C. Ahn, H. Peng, and H. E. Tseng, "Estimation of road friction for enhanced active safety systems: Dynamic approach," in *American Control Conference, 2009*, 2009, pp. 1110-1115.

[16] C. Ahn, H. Peng, and H. E. Tseng, "Robust nonlinear observer to estimate road friction coefficient and tire slip angle," in *10th International Symposium on Advanced Vehicle Control*, Loughborough, UK, 2010.

[17] T. Dieckmann, "Assessment of road grip by way of measured wheel variables," in *FISITA*, London, 1992.

[18] K. Yi, K. Hedrick, and S.-C. Lee, "Estimation of tire-road friction using observer based identifiers," *Vehicle System Dynamics,* vol. 31, pp. 233 - 261, 1999.

[19] S. L. Miller, B. Youngberg, A. Millie, P. Schweizer, and J. C. Gerdes, "Calculating longitudinal wheel slip and tire parameters using GPS velocity," in *American Control Conference*, Arlington, Virgina, USA, 2001, pp. 1800-1805.

[20] F. Gustafsson, "Slip-based tire-road friction estimation," *Automatica,* vol. 33, pp. 1087-1099, 1997.

[21] S. Sastry and M. Bodson, *Adaptive control: stability, convergence, and robustness*. Englewood Cliffs, N.J.: Prentice Hall, 1989.

[22] H. B. Pacejka, "Tyre brush model," in *Tyre and Vehicle Dynamics*, 2nd ed Oxford, U.K.: Elsevier, 2005, pp. 93-134.